Multibeam Antenna Based on Partially Reflecting Defected Metasurface

Jie Luo, Li Li, Jinrong Su, Runbo Ma, Guorui Han, and Wenmei Zhang, *Senior Member, IEEE*

***Abstract*—In this letter, a multibeam antenna based on metasurface (MS) is proposed. By employing the partially reflecting defected MS as the radiator, taking port 1 as an example, the beam with multiple sidelobes is focused in the direction of (3°, 33°) and the peak gain increases from 6.3 to 10.57 dBi. Also, a narrow beam with half-power beamwidth of 31° is obtained in a dimension of $1.5\lambda_0 \times 1.5\lambda_0$. When the antenna is fed from different ports separately, the beams are steered in different directions. Also, through inserting the vias between two-layer patches of the MS unit, the sidelobe is suppressed and the gain is improved. The results indicate that the antenna can operate at 7.5 GHz. When four ports are separately excited, the antenna can radiate four beams pointing at $(\varphi, \theta) =$ (3°, 33°), (93°, 33°), (183°, 33°), and (273°, 33°).**

***Index Terms*—Beam forming, metasurface (MS), multibeam antenna (MBA), vias.**

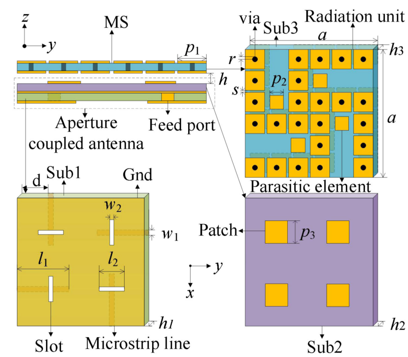

Fig. 1. Structure of the antenna.

I. Introduction

Multibeam antennas (MBAs) with fixed beam are widely used in wireless communication fields, especially where selective beam coverage is required [1]. Classic MBAs are based on beam-forming networks (BFN) and quasi-optical technology.

MBAs based on beam-forming circuits used power splitters, couplers, and phase shifters to generate an output signal with adjustable amplitude and phase, thereby realizing multiple beams [2], [3]. They maybe have a huge system footprint and a dramatically increased insertion loss caused by the BFN with the growing number of beams.

MBAs based on quasi-optical technology often were excited by plane waves and employed the transmissive or reflective metasurface (MS) as radiators [4]–[6]. In [6], the lens of the antenna has adopted a multilayer MS structure composed of Jerusalem cross elements and the realized antenna had a dimension of $10\lambda_0 \times 10\lambda_0 \times 5\lambda_0$. For this type of antenna, multifocal reflector/lens and long feeding distance would lead to a large dimension and high profile. Also, with substantially increased phase error and mutual coupling, the quality of beams can be severely deteriorated.

Manuscript received April 19, 2021; revised June 13, 2021; accepted June 17, 2021. Date of publication June 23, 2021; date of current version August 4, 2021. This work was supported in part by the National Science Foundation of China under Grant 62071282 and Grant 61775126; in part by Excellent Achievement Cultivation Project for Universities in Shanxi Province under Grant 2019KJ001; in part by the National Science Foundation of Shanxi Province under Grant 201901D111025; and in part by Shanxi "1331 Project" Key Subjects Construction under Grant 1331KSC. *(Corresponding author: Wenmei Zhang.)*

The authors are with the School of Physics and Electronics Engineering, Shanxi University, Taiyuan 030006, China (e-mail: 2867518676@qq.com; lili@sxu.edu.cn; sujinrong@sxu.edu.cn; marunbo@sxu.edu.cn; han_gr@sxu.edu.cn; zhangwm@sxu.edu.cn).

Digital Object Identifier 10.1109/LAWP.2021.3091608

Recently, the MBA using holographic techniques has attracted people's attention [7], [8]. They commonly operated in leaky-wave mode and etched on the circular dielectric with a larger radius of $10\lambda_0$–$12\lambda_0$.

In order to reduce the antenna volume and power consumption, MBAs without BFN were proposed in [9]–[15]. These antennas have compact areas and the maximum dimension of these antennas is $2.52\lambda_0 \times 2.52\lambda_0$. But the miniaturization also leads to wide beam and low gain.

In this letter, an MBA based on partially reflecting defected MS is proposed to achieve high directivity and narrow beam in a small area. The realized antenna has an impedance bandwidth from 7.45 to 7.57 GHz. Compared with the articles presented in [9]–[15], the novel antenna obtains the inclined narrower beam with half-power beamwidth (HPBW) of 31° and higher gain of 10.57 dBi in an area of $1.5\lambda_0 \times 1.5\lambda_0$ by loading the defected MS. Furthermore, the gain of the antenna is improved by arranging vias to connect the patches of the MS unit.

II. Design of Antenna

Fig. 1 shows the geometry of the proposed antenna. It includes the aperture coupled antenna and MS separated by an air cavity with a height of h. The aperture coupled antenna acts as the source of the entire antenna. It is composed of three metal layers, referred as the patch layer, the ground plane, and the feeding layer. The ground plane etched four slots and feeding layer having four microstrip lines are arranged on upper and lower sides of Sub 1 (FR-4 with $\epsilon_r = 4.4$ and tan $\delta = 0.02$), respectively. The patch layer formed by four square patches (with a side length $p_3 \approx 0.35\lambda g$, λg is the guided wavelength in the substrate) is fabricated on the Sub 2 (F4B with $\epsilon_r = 2.65$ and tan $\delta = 0.002$). The MS is etched on the upper and lower sides of Sub 3. Square patches are arranged in 6×6 arrays and the corresponding patches on two sides are connected through

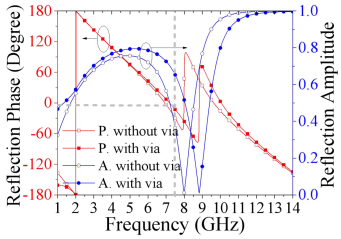

Fig. 2. Simulated reflection amplitude and phase of MS unit.

vias of radius r in the center. In order to improve radiation performance, the units located above the four microstrip feed units are removed and replaced with four parasitic patches. Then, the partially reflecting defected MS is formed. In addition, Subs 1–3 are all squares with a side length of $a \approx 6p_1 + 5s$. Finally, the antenna operating at 7.5 GHz is designed, and the optimized dimensions are given in Table I.

III. Characteristic of MS Unit and Design of Air Cavity

The MS unit is simulated using HFSS and results are shown in Fig. 2. For comparison, the result without via is also presented. Denote the reflection amplitude and phase of the unit with and without via as A_r, φ_r and A_{r0}, φ_{r0}, respectively. It is observed that φ_r and φ_{r0} are close except that around the frequency for zero reflection. Also, for the reflection amplitude, zero reflection appears at around 8 and 8.8 GHz for two cases. In the range of 2.5–8 GHz, $A_r > A_{r0}$ and A_r have a moderate value from 0.6 to 0.8. At 7.5 GHz, $A_{r0} = 0.36$ and $A_r = 0.65$. Therefore, the MS with vias is more fit as a partially reflecting surface.

Then, the air cavity is designed. It is known that when the height of the resonant cavity meets the condition, as given by (1), the electromagnetic wave will have an in-phase superposition in the resonant cavity [16]

$$H = (\varphi_r + \varphi_g)\frac{\lambda}{4\pi} \pm N\frac{\lambda}{2} \quad (N = 0,\ 1,\ 2,\ 3,\ldots). \tag{1}$$

Among them, φ_r and φ_g represent the reflection phase of the MS and ground plane, respectively. H is the height of the resonant cavity, and λ is the wavelength in the free space. It is known that $\varphi_r = -12.7°$ (see Fig. 2), $\varphi_g = 180°$, and

$$H = h + h_2 + h_3 \approx 9.3. \tag{2}$$

Then, the height h of the air cavity can be obtained as

$$h = 4.7. \tag{3}$$

After optimization, the h is determined as 4.8 mm.

IV. Multibeam Forming Technology

This section focuses on the beam-forming principle of the antenna. Without loss of generality, we take port 1 as an example to analyze. First, the aperture coupled antenna without MS is researched and its radiation pattern is shown in Fig. 3. Its maximum radiation direction is along the z-axis and the gain is 6.2 dBi. In order to tilt the beam and enhance its directivity, the defected MS is arranged. Also, patches formed the MS are connected through vias to suppress the sidelobe.

A. Evolution of Defected MS

In this section, the evolution of defected MS is discussed, and the corresponding result is indicated in Fig. 4. In Fig. 4(a), when

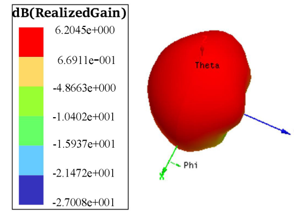

Fig. 3. Radiation patterns of aperture coupled antenna without MS at 7.5 GHz.

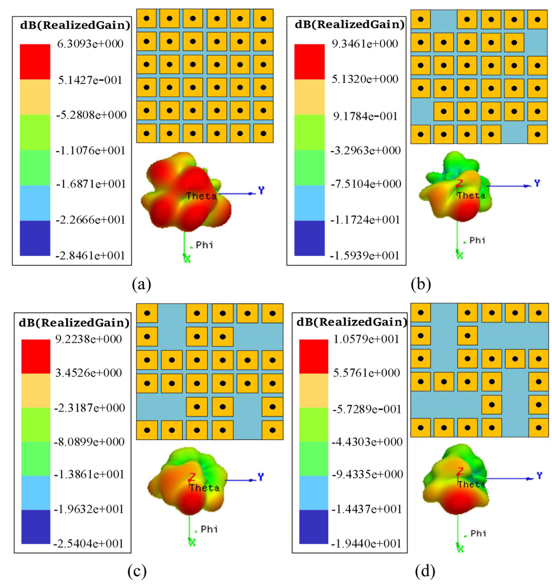

Fig. 4. Radiation patterns under different arrangements of MS. (a) Uniform MS. (b) Remove one MS unit. (c) Remove two MS units. (d) Remove three MS units.

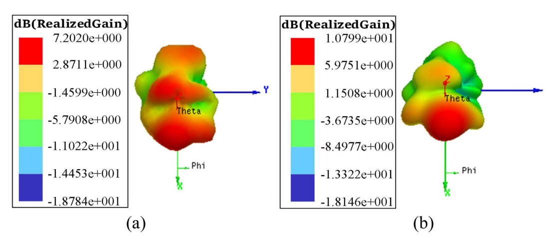

Fig. 5. Radiation patterns at 7.5 GHz. (a) MS without vias. (b) MS with vias.

a uniform MS is arranged, the beam has poor directivity, and multiple lobes scatter in different directions. The highest gain is 6.3 dBi. When one unit at each edge is removed, the directivity is improved, and the beam with the maximum gain of 9.34 dBi points at $(\varphi, \theta) = (20°, 33°)$, as shown in Fig. 4(b). In case that two sets of units are cut out, as revealed in Fig. 4(c), the beam is steered to $(\varphi, \theta) = (6°, 30°)$, and the gain reaches to 9.22 dBi. Finally, three sets of units are erased [see Fig. 4(d)]. As a result, the beam is directed at $(\varphi, \theta) = (3°, 33°)$, and the gain has been greatly improved to 10.57 dBi. From the above analysis, we can draw a conclusion that defected MS is helpful to improve the directivity and increase the gain.

B. Contribution of Vias

Then, the contribution of vias between the top and down patches of the MS unit will be illustrated. Fig. 5 shows the radiation patterns with and without vias. In Fig. 5(a), when the

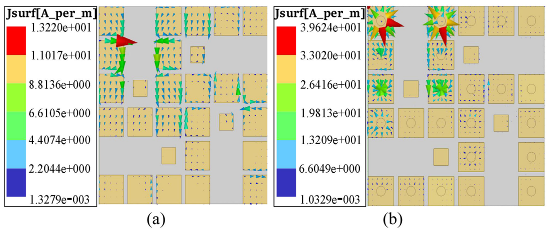

Fig. 6. Current distribution in MS. (a) Without vias. (b) With vias.

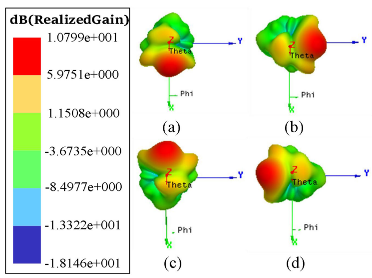

Fig. 7. Radiation patterns. (a) Port 1. (b) Port 2. (c) Port 3. (d) Port 4.

MS without vias is loaded, the beam is divided into three parts. Then, vias are loaded to connect two-layer MS, and the results are shown in Fig. 5(b). We can see that the beam has better directivity and lower sidelobe. Also, the gain reaches 10.79 dBi. The result can be discussed by analyzing the current distribution, as shown in Fig. 6. For the MS without vias, it is observed that the currents flow along the edges of the square patches, as shown in Fig. 6(a), which results in the scattered beams and high sidelobe level. After vias are arranged, as shown in Fig. 6(b), most of the currents on patches flow to or from the center. In this case, coupling between sides along the y-axis is weakened and the corresponding current (encircle with dotted line) is decreased. As a result, the directivity and gain are improved and the sidelobe is suppressed.

C. Forming Multibeams

When the ports 1–4 are excited separately, the antenna generates four different beams, as displayed in Fig. 7. It can be seen that four beams point at $(\varphi, \theta) = (3°, 33°)$, $(93°, 33°)$, $(183°, 33°)$, and $(273°, 33°)$. The beamwidth in the E- and H-plane are 31.11° and 59.79°, respectively. In addition, the gain is around 10.79 dBi.

V. Parameters Analysis

The proposed antenna is simulated using the HFSS and the effects of some geometric parameters are discussed in this section.

A. Influence of h and r

The height of the air cavity (h) has a larger influence on the radiation pattern. Fig. 8(a) shows the gain pattern in the $\varphi = 3°$ plane at 7.5 GHz for different h. When $h = 4.8$ mm, the antenna achieves a highest gain of 10.79 dBi and low sidelobe. In the case of $h = 2.8$ and 8.8 mm, the gain is reduced to 9.90 and 8.90 dBi, respectively. Fig. 8(b) shows the gain pattern in the $\varphi = 3°$ plane for different r. When $r = 1.5$ mm, the antenna has a gain of 10.79 dBi, HPBW of 31.11°, and the sidelobe level below 4.67 dB. As r increases or decreases, the gain decreases

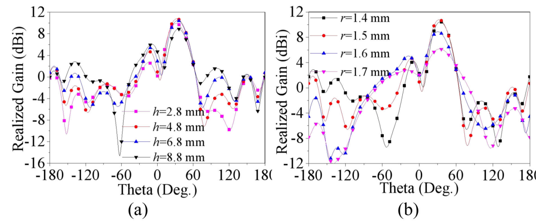

Fig. 8. Gain at 7.5 GHz for different parameters. (a) h. (b) r.

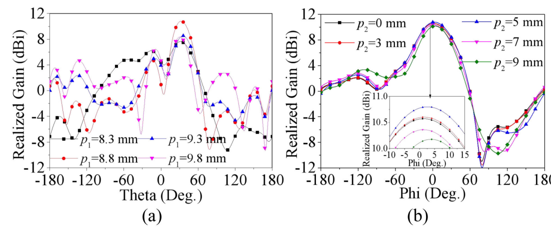

Fig. 9. Radiation pattern for different parameters. (a) p_1. (b) p_2.

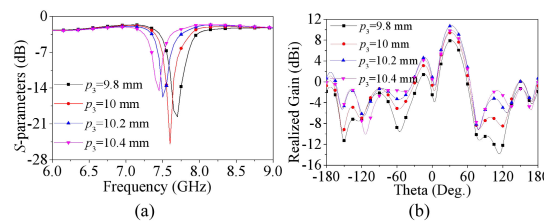

Fig. 10. Variations for different p_3. (a) S-parameters. (b) Gain.

and the sidelobe level increases. Especially when $r = 1.7$ mm, the gain decreases to 6.16 dBi, and the corresponding HPBW is 53.22°.

B. Effect of p_1 and p_2

The side length p_1 of the square patches formed the MS is also a major factor influencing the radiation pattern, as shown in Fig. 9(a). It can be found that, when $p_1 = 8.8$ mm, the antenna has the largest gain of 10.79 dBi and sidelobe level below 4.67 dB. In the case of $p_1 = 8.3$ mm, the gain decreases to 7.61 dBi and the sidelobe level increases to 6.20 dB. In the case of $p_1 = 9.3$ and 9.8 mm, similar phenomena can be observed. Thus, p_1 is chosen as 8.8 mm. Parasitic elements mainly affect the gain of the antenna. Fig. 9(b) shows the results for different p_2 at 7.5 GHz. When $p_2 = 0$ mm (there is no parasitic patch), the antenna has a gain of 10.51 dBi. If $p_2 = 5$ mm, the gain is increased to 10.79 dBi and an increment of 0.28 dBi is obtained. As p_2 increases to 9 mm, the sidelobe level has a slight increase and the gain decreases to 10.17 dBi. This indicates that the appropriate parasitic elements can improve the gain.

C. Effect of p_3

The side length p_3 of the patch printed on Sub 2 will affect the S-parameters and gain, as shown in Fig. 10. It can be found that the center frequency will decrease as p_3 increases. When $p_3 = 10.2$ mm, the resonant frequency is at 7.5 GHz and the corresponding maximum gain is 10.79 dBi. If p_3 changes, the gain will be decreased. Especially when $p_3 = 9.8$ mm, the gain is reduced to 7.95 dBi.

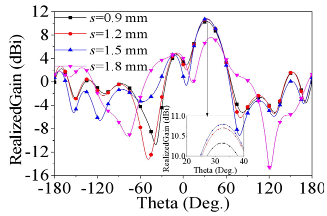

Fig. 11. Gain for different s.

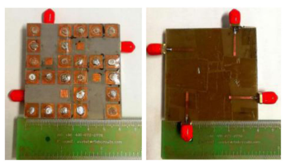

Fig. 12. Photographs of fabricated antenna.

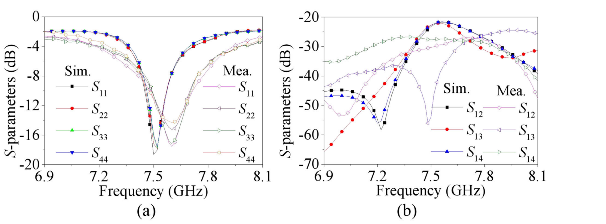

Fig. 13. S-parameters of the antenna. (a) Reflection parameters. (b) Isolation.

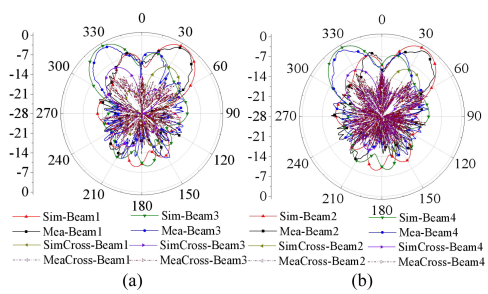

Fig. 14. Normalized radiation patterns at 7.5 GHz. (a) $\varphi = 3°$. (b) $\varphi = 93°$.

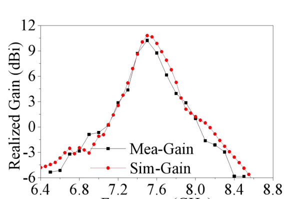

Fig. 15. Gain of the antenna at $\varphi = +3°$ and $\theta = 33°$.

D. Impact of s

The impact of the spacing between patches (s) on the radiation pattern is shown in Fig. 11. Compared with the case of $s = 1.5$ mm, with decrease of s, only the beam gain is slightly reduced by 0.5 dBi. But when s increases, the level of sidelobe is raised and the gain is lessened largely.

VI. Simulation and Measurement Results

In order to verify the design method, the prototype of the proposed antenna is fabricated, as shown in Fig. 12. Also, S-parameters, normalized radiation pattern, and gain are measured and the results are displayed in Figs. 13–15.

TABLE I
Optimized Parameters (Unit: mm)

Symbol	Quantity	Symbol	Quantity	Symbol	Quantity	Symbol	Quantity
a	60.3	p_1	8.8	p_2	5	p_3	10.2
w_1	1.5	w_2	1	l_1	18.1	l_2	5.8
h	4.8	h_1	1.6	h_2	1.6	h_3	3
r	1.5	d	13.95	s	1.5		

TABLE II
Comparison Between the Antenna and Reference Antennas

Antenna	Horizontal size	Beams number	Gain (dBi)	Frequency (GHz)	HPBW(°)
This paper	$1.5\lambda_0\times1.5\lambda_0$	4	10.79	7.5	31
[9]	$2.52\lambda_0\times2.52\lambda_0$	4	9.3	5.82	30
[11]	$0.94\lambda_0\times0.94\lambda_0$	4	9.1	4.7	70
[12]	$1.5\lambda_0\times1.5\lambda_0$	4	8.65	4.7	64.6

A. S-Parameters

The simulated and measured S-parameters of the proposed antenna are shown in Fig. 13. It should be noted that the isolation, when fed from other ports, is similar to that of port 1. Therefore, only the results for port 1 are provided. It could be found that the measured -10 dB impedance bandwidths for four ports are in the ranges of 7.46–7.71 GHz, 7.48–7.70 GHz, 7.48–7.71 GHz, and 7.46–7.71 GHz, respectively. Compared with the simulated results, the measured resonant frequency shifts 0.1 GHz, as displayed in Fig. 13(a). The differences between them are caused by fabrication errors. In Fig. 13(b), the measured isolation between the four ports is less than 25 dB, better than the simulated results of 20 dB.

B. Normalized Radiation Pattern

Fig. 14 shows the normalized radiation patterns of the antenna in the plane of $\varphi = 3°$ and $93°$ at 7.5 GHz. When the four ports are excited, respectively, the measured angle between the radiation beams and the z-axis is $33° \pm 2°$, and the corresponding simulated value is 33°. Also, the measured HPBW is 27.53°, which is 3.58° narrower than the simulated result of 31.11°. In addition, the measured cross level is less than 9 dB.

C. Gain

Fig. 15 shows the gain of the antenna when $\varphi = +3°$ and $\theta = 33°$. Considering the symmetry, only the results for port 1 are provided. It can be seen that the measured maximum value of 10.23 dBi appears at 7.5 GHz, which is 0.5 dBi lower than the simulated one.

Finally, Table II lists the characteristics of this and those reported MBAs. It is interesting to note that the antenna with defected MS achieves the highest gain and smaller beamwidth in comparable dimensions.

VII. Conclusion

An MBA based on MS has been designed in this letter. The partially reflecting defected MS covered above the aperture coupled antenna help to increase the gain and enhance the directivity. The measurement results show that the operating frequency of the antenna is around 7.5 GHz and four beams at an angle of $33° \pm 2°$ with regard to the z-axis can be obtained when exciting different ports, respectively. Correspondingly, the simulated gain of the main lobe can reach 10.79 dBi. It will display good application prospect in the field of wireless communication.

REFERENCES

[1] W. Hong *et al.*, "Multibeam antenna technologies for 5G wireless communications," *IEEE Trans. Antennas Propag.*, vol. 65, no. 12, pp. 6231–6249, Dec. 2017.

[2] Y. M. Cheng, P. Chen, W. Hong, T. Djerafi, and K. Wu, "Substrate-integrated-waveguide beamforming networks and multibeam antenna arrays for low-cost satellite and mobile systems," *IEEE Antennas Propag. Mag.*, vol. 53, no. 6, pp. 18–30, Dec. 2011.

[3] S.-J. Shi and W.-P. Ding, "Radiation pattern reconfigurable microstrip antenna for WiMAX application," *Electron. Lett.*, vol. 51, no. 9, pp. 662–664, Apr. 2015.

[4] L. Bao *et al.*, "Multi-beam forming and controls by metasurface with phase and amplitude modulations," *IEEE Trans. Antennas Propag.*, vol. 67, no. 10, pp. 6680–6685, Oct. 2019.

[5] Y. Hu, W. Hong, and Z. H. Jiang, "A multibeam folded reflectarray antenna with wide coverage and integrated primary sources for millimeter-wave massive MIMO applications," *IEEE Trans. Antennas Propag.*, vol. 66, no. 12, pp. 6875–6882, Dec. 2018.

[6] S. Li, Z. N. Chen, T. Li, F. H. Lin, and X. Yin, "Characterization of metasurface lens antenna for sub-6 GHz dual-polarization full-dimension massive MIMO and multibeam systems," *IEEE Trans. Antennas Propag.*, vol. 68, no. 3, pp. 1366–1377, Mar. 2020.

[7] D. González-Ovejero, G. Minatti, G. Chattopadhyay, and S. Maci, "Multibeam by metasurface antennas," *IEEE Trans. Antennas Propag.*, vol. 65, no. 6, pp. 2923–2930, Jun. 2017.

[8] M. Bodehou, E. Martini, S. Maci, I. Huynen, and C. Craeye, "Multibeam and beam scanning with modulated metasurfaces," *IEEE Trans. Antennas Propag.*, vol. 68, no. 3, pp. 1273–1281, Mar. 2020.

[9] J. Zhang, L. Han, X. Chen, R. Yang, and W. Zhang, "Multi-beam patch antenna based on metasurface," *IEEE Access*, vol. 8, pp. 37281–37286, 2020.

[10] D. Guan, Y. Zhang, Z. Qian, Y. Li, M. Asaadi, and C. Ding, "A novel 2-D multibeam antenna without beamforming network," *IEEE Trans. Antennas Propag.*, vol. 64, no. 7, pp. 3177–3180, Jul. 2016.

[11] A. Pal, A. Mehta, D. Mirshekar-Syahkal, and H. Nakano, "Low-profile steerable loop antenna with capacitively coupled feeds," *IEEE Antennas Wireless Propag. Lett.*, vol. 11, pp. 873–876, 2012.

[12] P. Deo, A. Mehta, D. Mirshekar-Syahkal, P. J. Massey, and H. Nakano, "Thickness reduction and performance enhancement of steerable square loop antenna using hybrid high impedance surface," *IEEE Trans. Antennas Propag.*, vol. 58, no. 5, pp. 1477–1485, May 2010.

[13] P. Lotfi, S. Soltani, and R. D. Murch, "Broadside beam-steerable planar parasitic pixel patch antenna," *IEEE Trans. Antennas Propag.*, vol. 64, no. 10, pp. 4519–4524, Oct. 2016.

[14] A. Grau Besoli and F. De Flaviis, "A multifunctional reconfigurable pixeled antenna using MEMS technology on printed circuit board," *IEEE Trans. Antennas Propag.*, vol. 59, no. 12, pp. 4413–4424, Dec. 2011.

[15] D. Rodrigo, Y. Damgaci, M. Unlu, B. A. Cetiner, J. Romeu, and L. Jofre, "Antenna reconfigurability based on a novel parasitic pixel layer," in *Proc. 5th Eur. Conf. Antennas Propag.*, 2011, pp. 3497–3500.

[16] D. R. Jackson *et al.*, "The fundamental physics of directive beaming at microwave and optical frequencies and the role of leaky waves," *Proc. IEEE*, vol. 99, no. 10, pp. 1780–1805, Oct. 2011.